Macroscopic trends of linear tearing stability in cylindrical current profiles

S Benjamin[1], C Clauser[1], C Rea[1], R Sweeney[2], A Kumar[1], E Marmar[1]

[1] Plasma Science and Fusion Center, MIT, Massachusetts Avenue, Cambridge, MA
[2] Commonwealth Fusion Systems, Hospital Rd, Devens, MA

E-mail: sbenjamin@psfc.mit.edu

Abstract. The likelihood of realising tokamak power-plants will be greatly improved by the discovery of high-gain equilibria that resist the formation of small islands and hence avoid the disruptive neoclassical tearing mode. However the complexity and variety of tearing-onset physics has obscured the design decisions that may lead to such stability. Here we investigate the variation that current profiles can bring about in preventing tearing onset through the cylindrical linear tearing stability parameter Δ'. A database of 159148 realistic pilot-plant current profiles was generated with Monte Carlo sampling, and the distribution of Δ' values was linked with interpretable profile characteristics. In agreement with prior theoretical and experimental studies, Δ' was found to be strongly correlated with the existence and steepness of a local toroidal current well or hill, with the former destabilising and the latter stabilising. In the absence of these two cases, the remaining Δ' values were linearly bounded by the toroidal current gradient at the rational surface.

Keywords: tearing mode, NTM seeding, Δ'
Submitted to: *Plasma Phys. Control. Fusion*

1. Introduction

Tearing modes in tokamaks are instances of magnetic reconnection that grow into magnetic islands. These islands can degrade energy confinement [1], lock with the plasma wall and lead to disruptions [1][2]. Once islands reach sizes greater than the perpendicular transport width (on the order of $\sim$ 1cm [3]) they can be driven towards further growth by the loss of local neoclassical bootstrap current, in an effect proportional to the local gradient in density and temperature [1][4]. As fusion rate scales with absolute density and temperature in the plasma [5][6], attempts to realise higher-gain tokamak plasma scenarios tend towards regimes of increasing instability through this mechanism. Accordingly, these bootstrap current-driven tearing modes (referred

to as neoclassical tearing modes or NTMs) [1][7] remain one of the chief physics risks that threaten the tokamak as a viable fusion power plant concept. Their occurrence has been observed across high-pressure tokamak scenarios including TFTR [8][9], JET [10], DIII-D [11] and ASDEX-U [12].

The mechanism driving NTM growth can be avoided if there are no seed-islands present to begin with [1]. Unfortunately, there are a variety of physics phenomena that govern tearing onset, including inherently unstable current profiles [13][14][15][16], pressure gradients at the rational surface [17][18], error fields [2][19][20], mode-coupling [21][22][23][24], seeding from other MHD activity [1][9][25] (including fast-ion driven instabilities [26]), and two-fluid effects like the generally stabilising [27] ion polarization current [1]. Some potential causes of tearing onset are unavoidable in high-gain tokamak equilibria, such as pressure gradients and MHD activity. Furthermore it is not always obvious in experimental observation which processes are dominant, as in the competing analyses of the ITER baseline scenario at DIII-D [11][16].

To simplify the picture we propose a series of studies linking the various tearing onset mechanisms to relevant aspects of machine design and operation. This will not only improve intuition about how to engineer greater passive NTM stability in tokamaks, but also provide mechanism-specific traits for future machine learning analyses of tearing-onset. In this work we investigate the potential stabilising effect that can be brought about by varying the plasma's current profile.

The tearability of different current profiles may be quantified in a cylindrical approximation using the Δ' term [13][18][28], which is inversely proportional to the magnetic energy cost of the reconnected mode in the small island limit [13][29]. Δ' is also the linear term in the nonlinear island growth equation or Modified Rutherford equation (MRE) [1][30]. If Δ' is large and negative, the critical island width at which neoclassical growth becomes dominant is increased [1]. Furthermore a negative-enough Δ' is predicted to provide stability regardless of the seeding island size [1][31]. While minimising Δ' should improve an equilibrium's robustness to NTM seeding [31], Δ' remains relatively un-intuitive as a stability parameter due to its calculation using energy-minimising global ideal-MHD perturbations [13][17].

In this study we attempt to understand Δ' through current profile features alone, with emphasis on maximally stable cases. A database of 159148 current profiles was generated with Monte Carlo sampling, for which Δ' was calculated with a finite-pressure asymptotic procedure. We found that the dominant characteristic of the most tearing-stable cases (negative Δ') was a local maximum in current density or 'current hill' at the mode rational surface. Local minima in current density or 'current wells' on the other hand were robustly destabilising. In the absence of these specific cases we observed Δ' could be bounded linearly by the negative toroidal current gradient at the rational surface, with $\Delta' < 0$ enforced by small enough gradients. Finally Δ' predictions of current well stability were validated using linear resistive MHD simulations in M3D-C1 [32].

This paper is organized as follows: Section 2 provides background on the mathematical treatment of the Δ' calculation, as well as the M3D-C1 simulations that were employed. Section 3 describes the processes used to generate the random database of cylindrical screw-pinch equilibria. Section 4 covers results of the database Δ' analysis, including identification of macroscopic trends in stability based on current-profile characteristics, and validation of Δ' stability predictions against M3D-C1 simulations. Section 5 provides a brief summary of these results in context of tearing literature, and addresses future work.

2. Background

In this section we will review the cylindrical Δ' calculation and its connection with linear tearing stability through asymptotic matching. This will provide the theoretical background necessary to repeat the Δ' tearing analysis we apply to the Monte Carlo equilibrium database.

Our tearing mode analysis begins by imposing a perturbation on a cylindrically symmetric background magnetic field $\mathbf{B} = B_z\hat{z} + B_\theta\hat{\theta}$. Note there is no radial component of $\mathbf{B}$ to ensure circularly nested flux surfaces. The background magnetic field is in static‡ force-balance with an input pressure profile p according to the following equilibrium relationships:

$$\frac{1}{2\mu_0}\frac{d}{dr}(B_z^2) = -\frac{dp}{dr} - B_\theta J_z, \tag{1}$$

$$\frac{1}{\mu_0}\frac{d(rB_\theta)}{dr} = rJ_z, \tag{2}$$

where B_z, B_θ, J_z and p are functions of r only.

Magnetic reconnection in our geometry requires plasma flow in the radial direction. For a plasma perturbation with resonant modal structure, these flows are strongly opposed everywhere except the mode rational surface, where the perturbation's structure aligns with the magnetic field [17] and the stabilising effect associated with field-line bending vanishes. Because of this globally suppressed radial flow, tearing only occurs at the rational surface, and the perturbation largely adheres to ideal MHD away from this point.

In linear tearing theory, the plasma perturbation is treated as ideal everywhere except a small distance δ either side of the rational surface, where resistive MHD is used to model reconnection [13][17][18]. Predictions about the tearing mode's stability, its corresponding energy, and its growth rate are made by locally matching numerically computed solutions of the ideal perturbation with analytic or numerical solutions to modes in the resistive 'inner' region [13][17][18][35]. This is done via equating asymptotic

‡ See [33][34] for cylindrical linear tearing theory in the presence of background flows.

forms of both solutions. To properly explain this process we will cover first ideal MHD perturbations (section 2.1) and their asymptotic form approaching the mode rational surface (section 2.2), and then resistive MHD perturbations (section 2.3) and their asymptotic form leaving the mode rational surface (section 2.4). Finally we will describe the asymptotic matching procedure and its consequences for stability prediction in section 2.5.

2.1. Ideal MHD perturbations far from the rational surface

The ideal-region component of the tearing mode is derived as follows: In a cylindrical plasma, with spatial periodicity mimicking a tokamak of major radius R_0 ('straight tokamak'), the energy of an internal ideal MHD plasma perturbation with Fourier structure is given by [36]

$$\delta W_F = \frac{2\pi^2 R_0}{\mu_0}\int_0^a (f\xi'^2 + g\xi^2)dr. \tag{3}$$

where ξ is the plasma displacement in the radial direction, and

$$\begin{aligned}
f(r) &= \frac{rF^2}{k_0^2},\\
g(r) &= 2\mu_0\frac{k^2}{k_0^2}\frac{dp}{dr} + \frac{k_0^2 r^2 - 1}{k_0^2 r^2}rF^2 + 2\frac{k^2}{rk_0^4}FF^\dagger,\\
k_0 &= k^2 + \frac{m^2}{r^2}\\
F(r) &\equiv \mathbf{k}\cdot\mathbf{B} = kB_z - \frac{mB_\theta}{r},\\
F^\dagger(r) &= kB_z + \frac{mB_\theta}{r}.
\end{aligned}$$

Here m and k are the perturbation's wavenumbers in the azimuthal and z-directions respectively. k is set to n/R_0 to replicate the toroidal periodicity of a tokamak.

A physical perturbation will minimise δW_F (3), and will therefore obey the Newcomb equation [36]:

$$\frac{d}{dr}\Big(f\frac{d\xi}{dr}\Big) - g\xi = 0 \tag{4}$$

which can be re-written in terms of the perturbed magnetic potential $\psi = \xi F$ as follows [13][37]:

$$\frac{d^2\psi}{dr^2} + \frac{1}{H}\frac{dH}{dr}\frac{d\psi}{dr} - \frac{1}{H}\Big[\frac{g}{F^2} + \frac{1}{F}\frac{d}{dr}\Big(H\frac{dF}{dr}\Big)\Big]\psi = 0,\ \ H = \frac{r^3}{n^2(r/R_0)^2 + m^2}. \tag{5}$$

If the safety factor $q \equiv \frac{rB_z}{R_0 B_\theta}$ is equal to a rational number m/n at some location r_s within the plasma, $F(r_s) = 0$ and the corresponding ideal mode described by equations (4) & (5) becomes singular approaching $r = r_s$. This is the rational surface at which non-ideal effects become important.

2.2. Asymptotic form of ideal perturbations approaching the rational surface

To match the ideal-region component of the tearing mode with a solution in the resistive region, we must first characterise the ideal solution near the rational surface, where it becomes singular.

Ideal-region solutions, described by equation (4), can be expressed as a Frobenius expansion in the vicinity of the singular point at the rational surface [28][38]. These solutions have the following form [28][29]:

$$\xi_\pm = |x|^{\sigma_\pm} \sum_{n=0}^{\infty} x^n \xi_{n\pm}, \tag{6}$$

$$\sigma_\pm = -1/2 \pm \sqrt{-D_I}, \tag{7}$$

$$\xi_{n\pm} = \frac{-\sum_{j=0}^{n-1} \xi_{j\pm}(f_{n+2-j}(\sigma_\pm + j)(\sigma_\pm + n + 1) - g_{n-j})}{f_2(\sigma_\pm + n)(\sigma_\pm + n + 1) - g_0}, \tag{8}$$

where $x = r - r_s$, $D_I = -1/4 - g_0/f_2$ is the Suydam stability criterion [39], ξ_0 is an arbitrary constant due to the homogeneous nature of equation (4), and

$$f_2 = \left(\frac{rF'^2}{k_0^2}\right)_{r_s}, \tag{9}$$

$$g_0 = \left(\frac{2\mu_0 k^2 p'}{k_0^2}\right)_{r_s}, \tag{10}$$

are the first non-zero terms in the Talyor expansions of f and g around r_s respectively:

$$f(r) = \sum_{m=0}^{\infty} f_m x^m = f_2 x^2 + O(x^3), \tag{11}$$

$$g(r) = \sum_{m=0}^{\infty} g_m x^m = g_0 + O(x). \tag{12}$$

In general, ξ near r_s is a linear combination of 'big' ξ_- and 'small' ξ_+ Frobenius solutions,

$$\xi = c(\xi_- + \Delta\xi_+), \tag{13}$$

where the energy of the big solution diverges at r_s while that of the small solution goes to 0 [39]. Δ is evaluated separately for either side of r_s by matching the asymptotic form of ξ to a numerical solution of equation (4). This is done with the following relations [29]:

Let

$$z_l \equiv \frac{\xi(r_s - \delta)}{\xi'(r_s - \delta)} = \frac{c_l(\xi_-(r_s - \delta) + \Delta_l \xi_+(r_s - \delta))}{c_l(\xi'_-(r_s - \delta) + \Delta_l \xi'_+(r_s - \delta))} \tag{14}$$

where Δ_l is the ratio Δ from equation (13) at $r = r_s - \delta$ ('left' of r_s). z_l is calculated from a numerical solution of equation (4). The ideal matching width $\delta > 0$ must be small enough to have good convergence of the asymptotic form with the numerical solution. However for asymptotic matching to be physically

relevant δ must be less than the resistive layer width (this is formalised in section 2.4). Rearranging equation (14), we have

$$\Delta_l = \frac{z_l \xi'_-(r_s-\delta) - \xi_-(r_s-\delta)}{\xi_+(r_s-\delta) - z_l \xi'_+(r_s-\delta)}. \tag{15}$$

z_r and Δ_r are defined the same as z_l and Δ_l except that they are evaluated at $r = r_s + \delta$.

The ratios of asymptotic forms of the ideal solutions Δ_l and Δ_r are the key information that the ideal-region provides for matching with resistive solutions and predicting the stability and growth rate of the tearing mode. In the cylinder, their sum [40] is equal to the logarithmic jump in the derivative of the perturbed magnetic potential:

$$\Delta' \equiv \frac{\psi'(r_s+\delta) - \psi'(r_s-\delta)}{\psi(r_s)} = \Delta_l + \Delta_r \tag{16}$$

which is inversely proportional to the ideal energy of the mode via [13][29]

$$\delta W_F = -H(r_s)\psi(r_s)^2 \Delta'. \tag{17}$$

2.3. Resistive MHD in the vicinity of the rational surface in cylindrical geometry

To match the ideal-region component of the tearing mode with the resistive-region solution, we must formulate the resistive solutions themselves. Accordingly, the following equations describe a generalised resistive MHD perturbation in toroidal geometry in the vicinity of the rational surface [18]:

$$\frac{d^2}{dx_i^2}\mathbf{\Psi} = \hat{\mathbf{U}} \cdot \mathbf{\Psi} + \hat{\mathbf{V}} \cdot \frac{d\mathbf{\Psi}}{dx_i} \tag{18}$$

where

$$\mathbf{\Psi} = [\tilde{B}_{1\perp}(x_i), \xi(x_i), \tilde{B}_{1\parallel}(x_i)], \tag{19}$$

$$\hat{\mathbf{U}} = \begin{pmatrix} Q & -x_i Q & 0 \\ -x_i/Q & x_i^2/Q & -(E+F)/Q^2 \\ -x_i/Q & -(G-KE)Q & x_i^2/Q + (G+KF)Q \end{pmatrix}, \tag{20}$$

$$\hat{\mathbf{V}} = \begin{pmatrix} 0 & 0 & H \\ -H/Q^2 & 0 & 0 \\ HKQ & 0 & 0 \end{pmatrix}, \tag{21}$$

and $Q = \gamma/Q_r$ and $x_i = (r - r_s)/L_r$ are the rescaled mode growth rate and rescaled inner region radial coordinate respectively, with scaling factors (cylindrical case [40])

$$L_r = \left[\frac{\rho_0 \eta^2 r_s^2}{n^2 B_\theta^2 q'^2}\right]_{r_s}^{1/6},$$

$$Q_r = \frac{\eta}{L_r^2}.$$

The background mass density is denoted by ρ_0, while η is a small, uniform plasma resistivity. In the cylinder H=0, and the remaining terms are defined as follows [40]:

$$\tilde{B}_{1\perp}(x_i) = \left(\frac{ir_s}{nB_\theta q' L_r}\right)_{r_s} B_{1r}(x_i),$$
$$\tilde{B}_{1\parallel}(x_i) = \left(\frac{-2Bk^2}{q'^2 B_\theta^2}\right)_{r_s} B_{1\parallel}(x_i),$$

where B_{1r} is the perturbed radial magnetic field component, $B_{1\parallel}$ is the perturbed magnetic field component parallel to the background magnetic field, and ξ is the perturbed radial plasma displacement as in the Newcomb equation (4). Finally

$$E + F = -\left(\frac{2p' r_s}{B_\theta^2 R^2 q'^2}\right)_{r_s},$$
$$F = \left(\frac{p'^2 r_s^2}{B_\theta^4 R^2 q'^2}\right)_{r_s},$$
$$K = \frac{1}{F},$$
$$G = \frac{1}{\Gamma}\left(\frac{B^2}{p}\right)_{r_s},$$

where Γ is the ratio of specific heats of the plasma.

The equations described above were derived in [41] & [18] in rationalized Gaussian units ($c = 1$) by linearising the resistive MHD equations around a stationary background state, assuming an eigenmode exponential time dependence $\propto \exp(\gamma t)$, applying a Lagrangian fluid displacement $\xi = (1/\gamma)\mathbf{v}$ and assuming the background equilibrium values are constant in the vicinity of the rational surface. The cylindrical case we apply here [40] also bears similarity to an adapted low-pressure slab treatment in [13].

2.4. Resistive MHD asymptotic forms leaving the rational surface

We wish to match the ideal-region component of the tearing mode with the resistive-region solution via their asymptotic forms. In this subsection we will see that the resistive inner region solution has the same asymptotic form as the ideal region solution as is necessary for asymptotic matching.

The resistive perturbation equation (18) possesses an irregular singular point at infinity, and solutions approach the following asymptotic form in the large x_i limit [18][29]:

$$\mathbf{\Psi} = \sum_{i=1\pm,2\pm,3\pm} \alpha_i \mathbf{\Psi_i}, \tag{22}$$

$$\mathbf{\Psi_{1\pm}} = |x_i|^{\sigma_{1\pm}} \begin{pmatrix} \sum_{n=-1}^{\infty} \psi_{n,1,1\pm} 1/x^n \\ \sum_{n=0}^{\infty} \psi_{n,2,1\pm} 1/x^n \\ \sum_{n=0}^{\infty} \psi_{n,3,1\pm} 1/x^n \end{pmatrix}, \tag{23}$$

$$\mathbf{\Psi_{2\pm}} = \exp\left(\frac{x_i^2}{2\sqrt{Q}}\right)|x_i|^{\sigma_{2\pm}} \begin{pmatrix} \sum_{n=1}^{\infty} \psi_{n,1,2\pm} 1/x^n \\ \sum_{n=0}^{\infty} \psi_{n,2,2\pm} 1/x^n \\ \sum_{n=0}^{\infty} \psi_{n,3,2\pm} 1/x^n \end{pmatrix}, \tag{24}$$

$$\mathbf{\Psi_{3\pm}} = \exp\left(-\frac{x_i^2}{2\sqrt{Q}}\right)|x_i|^{\sigma_{3\pm}} \begin{pmatrix} \sum_{n=1}^{\infty} \psi_{n,1,3\pm} 1/x^n \\ \sum_{n=0}^{\infty} \psi_{n,2,3\pm} 1/x^n \\ \sum_{n=0}^{\infty} \psi_{n,3,3\pm} 1/x^n \end{pmatrix}, \tag{25}$$

where solutions $\mathbf{\Psi_{2\pm}}$ and $\mathbf{\Psi_{3\pm}}$ possess exponentially growing and decaying "controlling factors"[42] respectively§. Note in fusion plasmas the large x_i limit is consistent with the size of a small island because resistivity (and hence L_r) is small [43].

To observe finite amplitude perturbations the exponentially growing solution must be eliminated by enforcing $\alpha_{2\pm} = 0$. Furthermore at large x_i the exponentially decaying solution becomes negligible, and we are left with a linear combination of $\mathbf{\Psi_{1\pm}}$ solutions where

$$\sigma_{1\pm} = -\frac{1}{2} \pm \sqrt{\frac{1}{4} - (E+F)} = -\frac{1}{2} \pm \sqrt{-D_I} = \sigma_{\pm}. \tag{26}$$

At 0th order these solutions have an identical mathematical form to the 0th order ideal region solutions in equation (6):

$$\xi = c_-|x|^{\sigma_-} + c_+|x|^{\sigma_+}. \tag{27}$$

This similarity of asymptotic forms is what makes the asymptotic matching process possible, provided that there is a region of overlap where both the 0th order solutions of the ideal and resistive perturbations are good approximations of their full solutions. This overlap criteria may be quickly checked by confirming whether the following relationships are true [40]:

$$\tau_A \gamma \ll 1, \;\; Q \gg 1,$$
$$\gamma \gg \eta/(\mu_0 r_s^2), \;\; Q \ll 1,$$

where $\tau_A = r_s[\sqrt{4\pi\mu_0\rho_0}/B]_{r_s}$ is the local Alfven time. Alternatively one can calculate the characteristic resistive layer width [43]:

$$\delta r = \left[\rho_0 \left(\frac{\eta R}{nB}\frac{q}{q'}\right)^2_{r_s}\right]^{\frac{1}{6}} |Q|^{\frac{1}{4}} \tag{28}$$

and check that the ideal region 0th order asymptotic solution is well-converged within a distance $\delta > \delta r$ from the rational surface. In the limit of zero resistivity these overlap criteria will always be satisfied, however they must still be checked for thermonuclear plasmas [24].

§ See [29] for an explicit derivation of these exponential controlling factors.

2.5. Tearing stability and growth rate predictions from asymptotic matching

Now that we have descriptions of the mode structure in both the ideal and resistive regions, we can connect them through their matching asymptotic forms and predict the tearing-mode's stability and growth rate.

The asymptotic matching procedure is done by equating the ratios of big and small solutions ($\Delta = c_+/c_-$) of the zeroth order asymptotic forms of the inner and outer region solutions on either side of the rational surface. Glasser et al. [18] derived an analytic approximation of the inner region asymptotic solution during matching to arrive at the following dispersion relation (cylindrical case):

$$\Delta' = \frac{2\pi}{L_r}\frac{\Gamma(\frac{3}{4})}{\Gamma(\frac{1}{4})}Q^{5/4}(1 - \pi D_R/4Q^{3/2}) \tag{29}$$

where D_r is proportional to the local pressure gradient via [18][40]

$$D_R = -2p'r_s/(B_\theta^2 R^2 q'^2)|_{r_s}. \tag{30}$$

An analysis of this dispersion relation shows that if $D_R > 0$ we always have a pressure-driven instability called the resistive interchange mode [18]. For $D_R = 0$, however, the growth rate Q is proportional to $\Delta'^{4/5}$ such that if $\Delta' > 0$ we are tearing-unstable and if $\Delta' < 0$ we are tearing-stable. Finally for $D_R < 0$, there is some critical $\Delta_C \approx (1.54/L_r)|D_R|^{\frac{5}{6}} > 0$ where we are tearing unstable for $\Delta' > \Delta_C$, and stable otherwise [18].

Numerical solutions to the inner region equations can also be used to calculate the inner region ratios ($\Delta = c_+/c_-$) [24][29][35][40][44], providing greater accuracy than the approximate analytic methods of [24]. See [40] for an instructive example in cylindrical geometry. Numerical matching has been shown to closely predict tearing-mode growth rates when compared to linearised resistive MHD treatments in toroidal [24] and cylindrical geometry [29][40]. However this procedure requires repeatedly solving the inner equations in a complex root-finding loop [24], complicating its unsupervised application at large scales. We leave the implementation of numerical inner-region matching to a future toroidal continuation of this study.

3. Method

In this section we will explain the Monte Carlo method we employed to generate a database of realistic straight tokamak equilibria. This database was intended to exhaust the space of current profiles that might reasonably occur in a tokamak pilot-plant, allowing us to observe any beneficial current-profile effects on tearing stability. Due to our use of a straight tokamak geometry, the 'z' & 'θ' directions going forward will be referred to as the 'toroidal' (subscript t) and 'poloidal' (subscript p) directions respectively.

3.1. General cubic spline cylindrical equilibria

A flexible spline-based cylindrical equilibrium code was written to calculate straight tokamak equilibria from randomly generated current profiles. The equilibrium solver was completely characterised by an input toroidal current profile, input pressure profile and toroidal magnetic field strength at some reference r. The toroidal current was prescribed the form of a cubic spline as follows:

$$J_t(r) = a_i(r-r_i)^3 + b_i(r-r_i)^2 + c_i(r-r_i) + d_i \equiv P_i^{(3)}(r) \tag{31}$$

for r between spline 'knots' $r_i \leq r < r_{i+1}$, while the pressure profile's only requirement was an analytic description of its derivative.

The poloidal magnetic field $B_p(r)$ was found by integrating successive intervals of the cubic spline as follows:

$$\begin{aligned} B_p(r) &= \frac{\mu_0}{r}\int_0^r r' J_t(r')dr' \\ &= \frac{\mu_0}{r}\left[\sum_{i=1}^{j-1}\int_{r_i}^{r_{i+1}} r' P_i^{(3)}(r')dr' + \int_{r_j}^{r} r' P_j^{(3)}(r')dr'\right] \qquad (32) \\ &\equiv \frac{\mu_0}{r}\left[M_j + I_j^{(5)}(r)\right] \qquad (33) \end{aligned}$$

for $r_j \leq r < r_{j+1}$, where

$$\begin{aligned} I_i^{(5)}(r) &\equiv \int_{r_i}^{r} dr'\, r' P_i^{(3)}(r') \qquad (34) \\ &= \frac{a_i}{5}r^5 + \frac{b_i - 3a_i r_i}{4}r^4 + \left[\frac{c_i - 2b_i r_i}{3} + a_i r_i^2\right]r^3 + \frac{d_i - c_i r_i + b_i r_i^2 - a_i r_i^3}{2}r^2, \\ M_j &= \int_0^{r_j} r J_t(r)dr - I_j^{(5)}(r_j) = \sum_{i=1}^{j-1}[I_i^{(5)}(r_{i+1}) - I_i^{(5)}(r_i)] - I_j^{(5)}(r_j), \qquad (35) \end{aligned}$$

and $M_0 = M_1 = 0$.

The toroidal magnetic field $B_t(r)$ was found by pre-calculating analytic spline integral combinations and summing them over successive intervals of increasing radius:

$$B_t(r) = \sqrt{B_t(r_{ref})^2 - 2[p(r) - p(r_{ref})] - 2\mu_0\int_{r_{ref}}^{r} B_p(r')J_t(r')dr'}, \tag{36}$$

where

$$\int_0^r B_p(r')J_t(r')dr' = \sum_{i=1}^{j-1}[O_i + P_i] + M_j\left[L_j^{(3)}(r) - L_j^{(3)}(r_j)\right] + K_j^{(8)}(r) - K_j^{(8)}(r_j) \tag{37}$$

for $r_j \leq r < r_{j+1}$. The sub-components I and M are given by equations (34) and (35) respectively, while L, K, O and P are defined as follows:

$$\begin{aligned} L_i^{(3)}(r) &\equiv \int_{r_i}^{r}\frac{1}{r'}P_i^{(3)}(r')dr' \\ &= \frac{a_i}{3}r^3 + \frac{b_i - 3a_i r_i}{2}r^2 + (c_i - 2b_i r_i + 3a_i r_i^2)r + (d_i - c_i r_i + b_i r_i^2 - a_i r_i^3)\ln(r), \end{aligned}$$

$$
\begin{aligned}
K_i^{(8)}(r) \equiv & \int_{r_i}^{r} \frac{1}{r'} I_i^{(5)}(r') P_i^{(3)}(r') dr' \\
= & \frac{a_i^2}{40} r^8 + \left[\frac{9 b_i a_i}{140} - \frac{27 a_i^2 r_i}{140} \right] r^7 + \left[\frac{b_i^2}{24} + \frac{4 c_i a_i}{45} - \frac{77 b_i a_i r_i}{180} + \frac{77 a_i^2 r_i^2}{120} \right] r^6 + \\
& \left[\frac{7 c_i b_i}{60} + \frac{7 d_i a_i}{50} - \frac{7 b_i^2 r_i}{30} - \frac{49 c_i a_i r_i}{100} + \frac{119 b_i a_i r_i^2}{100} - \frac{119 a_i^2 r_i^3}{100} \right] r^5 + \\
& \left[\frac{c_i^2}{12} + \frac{3 d_i b_i}{16} - \frac{25 c_i b_i r_i}{48} - \frac{9 d_i a_i r_i}{16} + \frac{25 b_i^2 r_i^2}{48} + \frac{17}{16} c_i a_i r_i^2 \right. \\
& \left. - \frac{7}{4} b_i a_i r_i^3 + \frac{21 a_i^2 r_i^4}{16} \right] r^4 + \\
& \left[\frac{5 d_i c_i}{18} - \frac{5 c_i^2 r_i}{18} - \frac{5 d_i b_i r_i}{9} + \frac{5}{6} c_i b_i r_i^2 + \frac{5}{6} d_i a_i r_i^2 - \frac{5 b_i^2 r_i^3}{9} \right. \\
& \left. - \frac{10}{9} c_i a_i r_i^3 + \frac{25}{18} b_i a_i r_i^4 - \frac{5 a_i^2 r_i^5}{6} \right] r^3 + \\
& \left[\frac{d_i^2}{4} - \frac{d_i c_i r_i}{2} + \frac{c_i^2 r_i^2}{4} + \frac{1}{2} d_i b_i r_i^2 - \frac{1}{2} c_i b_i r_i^3 - \frac{1}{2} d_i a_i r_i^3 + \frac{b_i^2 r_i^4}{4} \right. \\
& \left. + \frac{1}{2} c_i a_i r_i^4 - \frac{1}{2} b_i a_i r_i^5 + \frac{a_i^2 r_i^6}{4} \right] r^2, \qquad (38)
\end{aligned}
$$

$$
O_i = \int_{r_i}^{r_{i+1}} \frac{1}{r'} M_i J_t(r') dr' = M_i \Big[L_i^{(3)}(r_{i+1}) - L_i^{(3)}(r_i) \Big], \qquad (39)
$$

$$
P_i = \int_{r_i}^{r_{i+1}} \frac{1}{r'} I_i^{(5)}(r') J_t(r') dr' = K_i^{(8)}(r_{i+1}) - K_i^{(8)}(r_i). \qquad (40)
$$

Finally the poloidal current density was calculated with

$$
J_p(r) = -\frac{1}{\mu_0} \frac{dB_t(r)}{dr} \qquad (41)
$$

$$
= \frac{1}{\mu_0} \frac{p'(r) + B_p(r) J_t(r)}{B_t(r)}. \qquad (42)
$$

3.2. Reference scenario for Monte Carlo equilibria database

The Monte Carlo cylindrical equilibrium database was developed to investigate maximally negative Δ' cases that may be applicable to future tokamak pilot plant equilibria. Accordingly, the random equilibria were based around a scaled-up SPARC-like [45] equilibrium, with macroscopic parameters outlined in table 1 and profiles plotted in figure 1.

The same peaked parabolic pressure profile seen in figure 1 was used for all equilibria in the database. This was done because a peaked pressure profile will always destabilise the cylindrical resistive interchange mode (see section 2.5), limiting the usefulness of pressure-profile scans.

Table 1. Reference scenario

Parameter	Value	Machine reference (approx.)
B_t on axis	12T	SPARC
q95	3.3	SPARC
I_{tot}	5.9MA	-
R_0	3m	JET/ARC
a	1m	JET/ARC
$\beta = 2\mu_0 p/B^2$	1% (axis)	SPARC

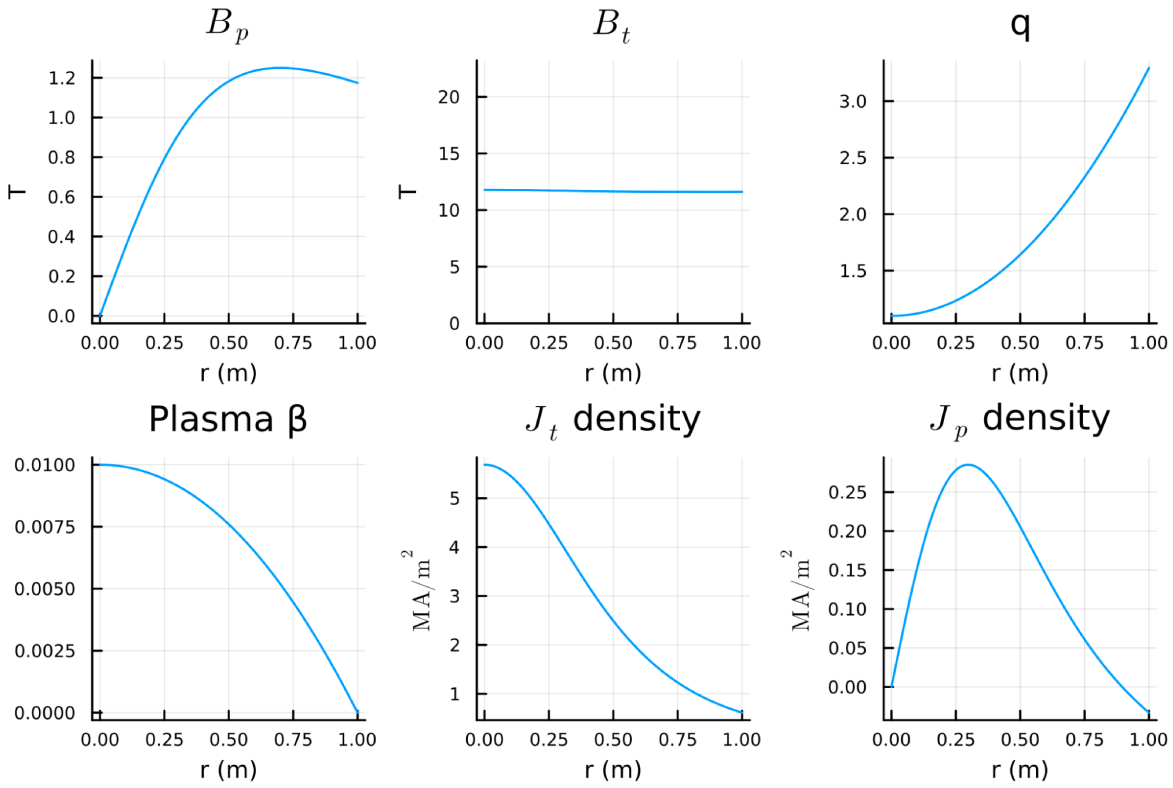

Figure 1. Equilibrium profiles of reference scenario

3.3. Monte Carlo sampling and constraints

To generate sufficiently diverse current profiles, spline knot locations $\{r_i\} \in [0, 1]$, knot number and knot values $\{J_t(r_i)\}$ were all randomly varied. Knot number was uniformly Monte Carlo (MC) sampled over the range 5-9, with knot location MC sampled from a peaked ($\alpha = 10$) Dirichlet distribution [46].

Edge J_t values were MC sampled from the following ranges:

$$J_t(0.0) \in [0.5J_{\text{t,ref}}, 1.2J_{\text{t,ref}}],$$
$$J_t(1.0) \in [0.0, 0.3J_{\text{t,ref}}],$$

where $J_{\mathrm{t,ref}} = J_{\mathrm{t,ref}}(0.0) = 5.7\mathrm{MAm}^{-2}$. Internal $J_t(r_i)$ values were MC sampled over the range $[0.0, J_t(0.0)]$ subject to the following constraints:

- Limit placed on absolute gradient $|J_t'| < 2J_{\mathrm{t,ref}}/a^2$.
- Gradient could only change sign 3 times.
- Total current I_{tot} was restricted (0.9-1.1 of reference equilibrium value).
- One rational surface for 2/1, 3/1 modes.

The aforementioned limits on absolute current gradient and gradient sign-changes removed extreme and unrealistic current profiles. We also ensured the remaining equilibria were ideal MHD stable by applying Suydam's criteria & Newcomb's procedure [39].

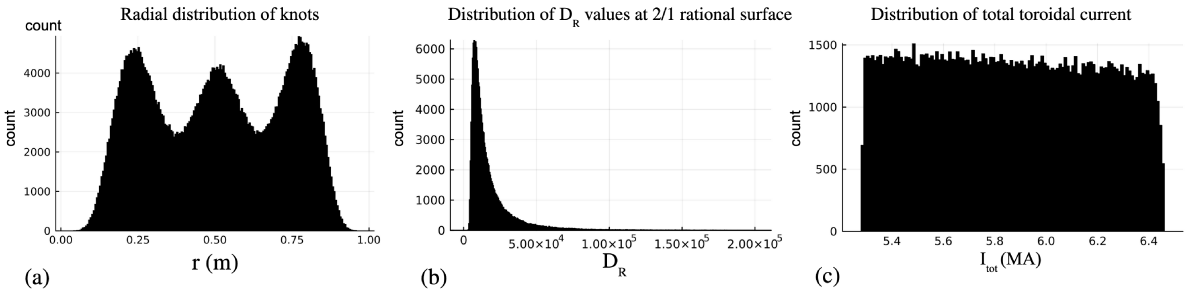

Figure 2. Equilibrium database distributions of spline knots (a), the resistive interchange criterion D_R (b) defined in equation (30), and total toroidal current I_{tot} (c).

These sampling methods resulted in an equilibrium database comprised of approximately 123000 5-knot equilibria, 23000 6-knot equilibria, and 11000 7-knot equilibria. The distribution of knot locations is shown in figure 2a, and is dense throughout the plasma volume as desired. All database values of the resistive interchange criterion D_R (30) were positive as expected of a peaked pressure profile. The distribution of D_R is shown in figure 2b. Finally the distribution of total current I_{tot} was well-constrained and approximately flat, as shown in figure 2c.

4. Results

In this section we describe the cylindrical equilibrium database's Δ' distribution, and its relation to relevant current profile characteristics. Statistical correlations with Δ' were quantified using the Spearman rank-order coefficient [47] 'r_{spear}'.

The distribution of rational surfaces r_s in the equilibrium database is displayed in figure 3. The corresponding 2D histograms of Δ' vs r_s for the 2/1 and 3/1 modes are displayed in figure 4. As can be seen in 4b, the 3/1 mode is strongly stabilised as $r_s \to 1\mathrm{m}$. This is a consequence of our choice of internal mode analysis, equivalent to

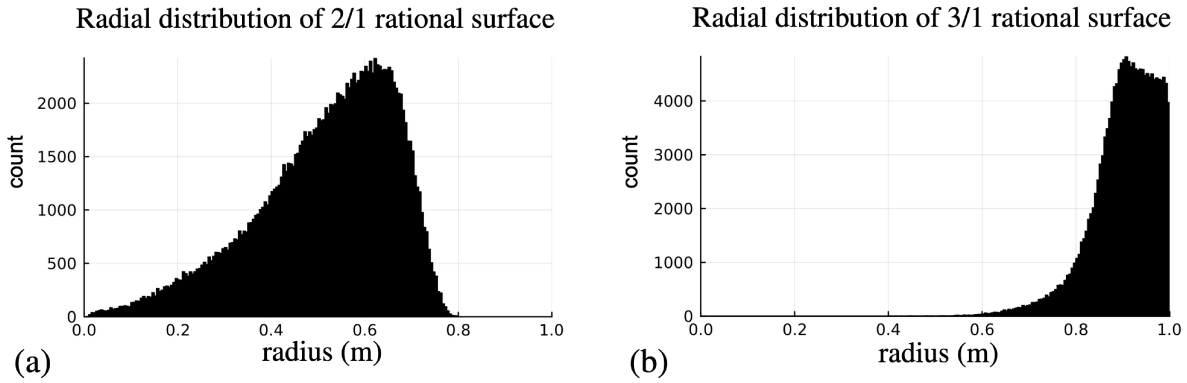

Figure 3. Equilibrium database histograms of the 2/1 and 3/1 rational surfaces.

the presence of an ideal wall at $r = 1$m. The 2/1 mode also displays an r_s dependence in 4a, being robustly destabilised as $r_s \to 0$ for $r_s < 0.3m$. These particular cases correspond with overly flat current profiles that differed significantly from the reference scenario q-profile. The observed 2/1 destabilisation as $r_s \to 0$ did not occur for other modes such as 3/2 and 4/3, meaning this is not a general effect. Accordingly, subsequent analysis will focus solely on 2/1 stability for $r_s > 0.3$m.

The database distribution of Δ' for 2/1 modes with $r_s > 0.3$m is displayed in figure 5. Note the majority of current profiles are unstable, with only 8% having $\Delta' < 0$. The 10 most stable current profiles, with Δ' values between -27 and -19, are plotted in figure 6a. They all share the characteristic of the rational surface lying on a local maximum in current density, or a 'current hill'. The 10 most unstable current profiles, with Δ' values between 97 and 120, are plotted in figure 6b. They all share the characteristic of the rational surface lying at a point of large local negative gradient in toroidal current density.

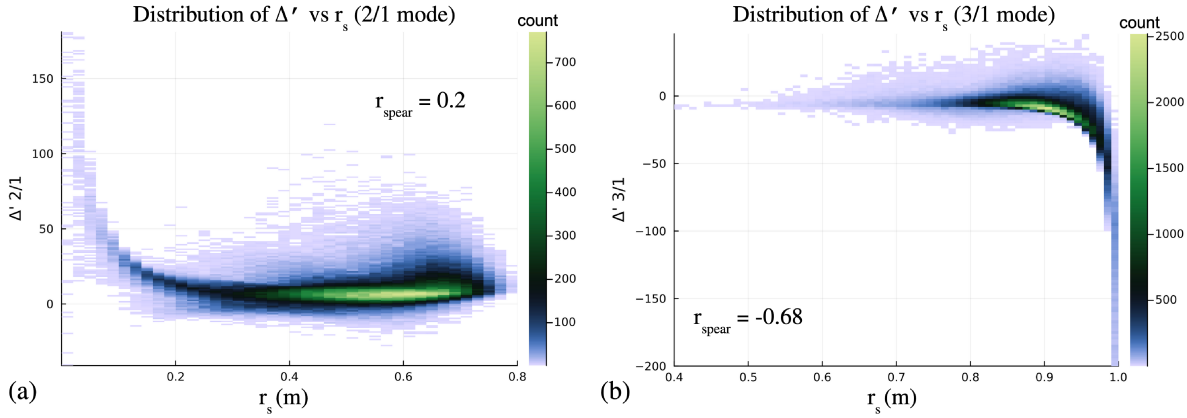

Figure 4. 2D histograms of Δ' vs r_s for the 2/1 (a) and 3/1 (b) modes.

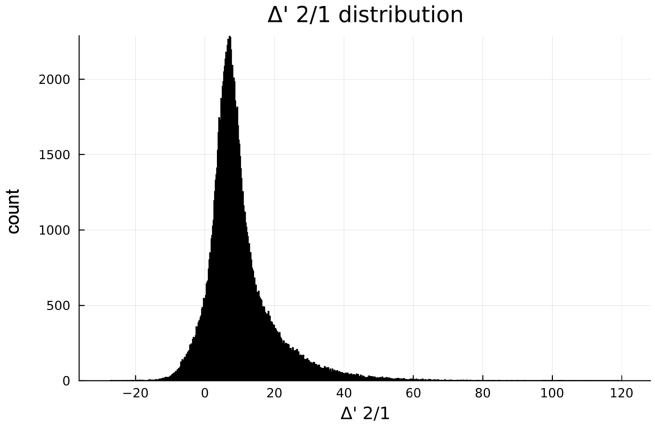

Figure 5. Histogram of Δ' for 2/1 modes with $r_s > 0.3$m.

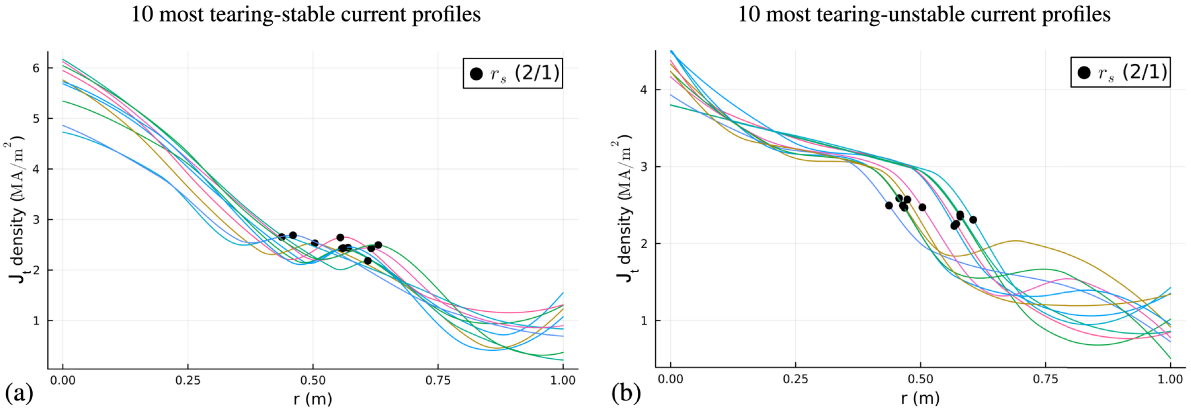

Figure 6. Figure (a) plots the 10 most stable current profiles in the database, with $\Delta' \in [-27, -19]$. Figure (b) plots the 10 most unstable current profiles, with $\Delta' \in [97, 120]$.

To quantify the stabilising properties of the current hill introduced in figure 6a, a hill-steepness parameter '$J_t/J_{t,hill}$' was defined as follows:

$$\nabla J_t/J_{t,hill} = \frac{[\min(h_1, h_2)/w]}{J_t(r_s)}, \tag{43}$$

where w is the distance from r_s to the inboard minimum point, h_1 is the height of the hill at r_s and $h_2 = J_t(r_s) - J_t(r_s + w)$. An illustration of these terms is provided in figure 7b.

Hill steepness has a strong negative correlation with Δ' as shown in figure 7a. The data-points in 7a are composed of 135 current profiles in the database that had the rational surface located near the peak of a current hill with $|r_s - r_{\text{local max}}| < 8$mm. Note the somewhat arbitrary value of $|r_s - r_{\text{local max}}| < 8$mm was chosen to classify local current hills because larger cutoff values of $|r_s - r_{\text{local max}}|$ decreased the strength of the correlation. This was presumably because r_s was no longer close enough to the center of the hill. Decreasing the cutoff from 8mm, on the other hand, started removing

data-points without notably changing r_{spear}.

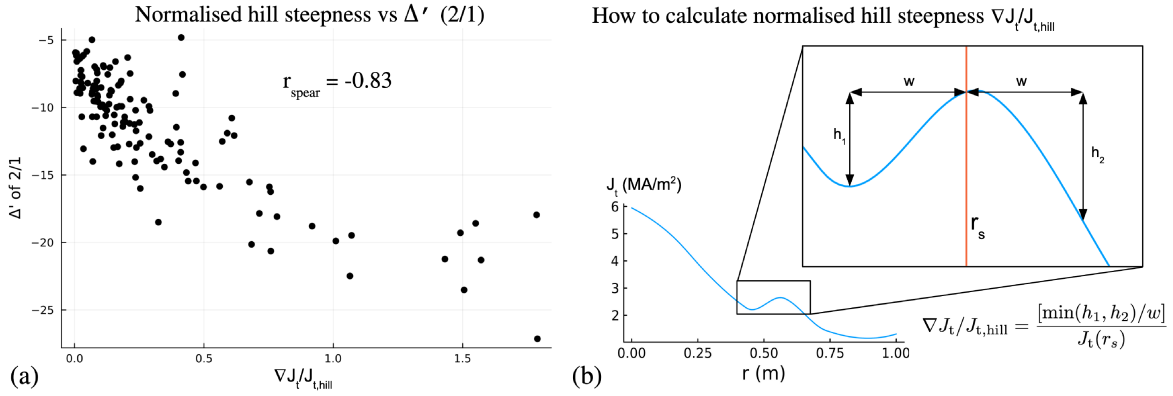

Figure 7. Figure (a) shows the relationship between Δ' and hill steepness $\nabla J_{\text{t}}/J_{\text{t,hill}}$, for 2/1 modes with r_s centered within 0.008m of the hill max point. Figure (b) shows how to calculate $\nabla J_{\text{t}}/J_{\text{t,hill}}$.

A well steepness parameter '$J_{\text{t}}/J_{\text{t,well}}$' was also defined by:

$$\nabla J_{\text{t}}/J_{\text{t,well}} = \frac{[\min(h_3, h_4)/w]}{J_{\text{t}}(r_s)}, \tag{44}$$

where w here is the distance from r_s to the outboard maximum point, h_3 is the depth of the well at r_s and $h_4 = |J_{\text{t}}(r_s) - J_{\text{t}}(r_s - w)|$. An illustration of $J_{\text{t}}/J_{\text{t,well}}$ is provided in figure 8b. Well steepness was strongly positively correlated with Δ' as shown in figure 8a. The data-points in figure 8a were composed of 498 current profiles in the database that had the rational surface near a local minimum $r_{\text{local min}}$ such that $|r_s - r_{\text{local min}}| < 8$mm. Like with the hill, the cutoff value of $|r_s - r_{\text{local min}}|$ was made small enough to maximise the strength of the correlation r_{spear} without needless excluding wells from the analysis.

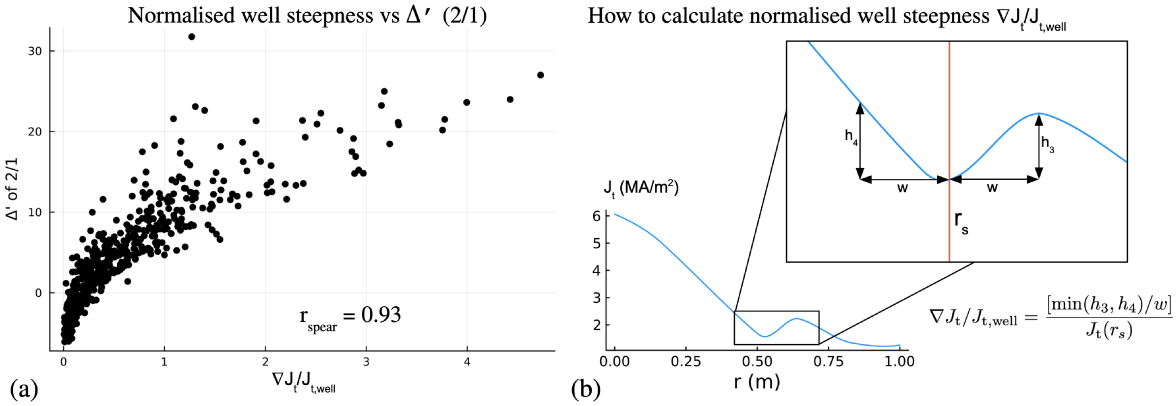

Figure 8. Figure (a) shows the relationship between Δ' and well steepness $\nabla J_{\text{t}}/J_{\text{t,well}}$, for 2/1 modes with r_s centered within 0.008m of the well max point. Figure (b) shows how to calculate $\nabla J_{\text{t}}/J_{\text{t,well}}$.

It is interesting to note that as well-steepness goes to zero, Δ' reliably transitions from positive to negative. This is because a very shallow well is just a region of small local current gradient, which is stabilising as we'll see in the following analysis:

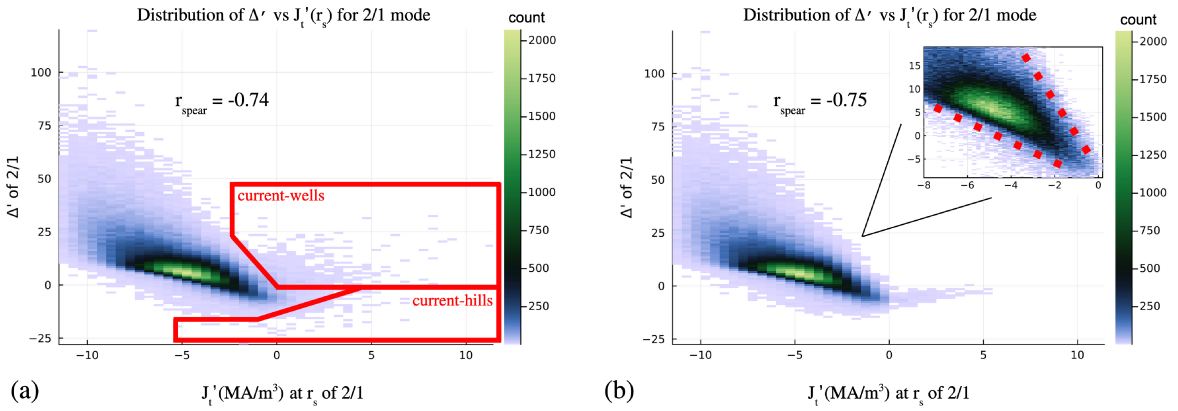

Figure 9. 2D histogram of Δ' vs $J'_t(r_s)$ for 2/1 modes with $r_s > 0.3$m. All cases where the rational surface lies in a current-well or current-hill have been removed in figure (b).

Figure 9a shows a 2D histogram of Δ' vs the local gradient in the toroidal current profile for 2/1 modes with $r_s > 0.3m$. It is clear a large negative gradient is robustly destabilising, while local current gradients close to 0 appear stabilising in the majority of cases. Furthermore if we remove all instances where the rational surface lies in a current well or current hill, as in figure 9b, Δ' can be bounded linearly above and below by J'_t, with $J'_t \approx 0$ ensuring $\Delta' < 0$.

Non-dimensionalising figure 9 by plotting $r_s\Delta'$ against $r_s J'_t(r_s)/J_t(r_s)$ caused minimal changes in the distribution shape, and reduced the negative magnitude of r_{spear} from -0.75 to -0.73.

Figure 10 compares the 2D histograms of Δ' vs magnetic shear q' and Δ' vs q'', to that of Δ' vs J_t and J'_t. We can observe that the Δ' dependence of q' and q'' is inversely related to that of J_t and J'_t, respectively. This is because the radial dependence of q is dominated by the poloidal field B_p which is the integral of J_t:

$$B_p \propto \frac{1}{r}\int r J_t.$$

The toroidal magnetic field $B_t(r)$, on the other hand doesn't significantly contribute to q', q'' since it is approximately constant due to the high background field and low β (illustrated in the figure 1 plot of B_t).

Figure 11 shows 2D histograms between Δ' and r_s, $p(r_s)$ and $p'(r_s)$. As the Δ' dependence of $p(r_s)$ and $p'(r_s)$ appear equal and opposite to that of r_s (including equal and opposite r_{spear} values), we can deduce that for our equilibrium database, local pressure and pressure gradient have no correlation with Δ' except through their mutual

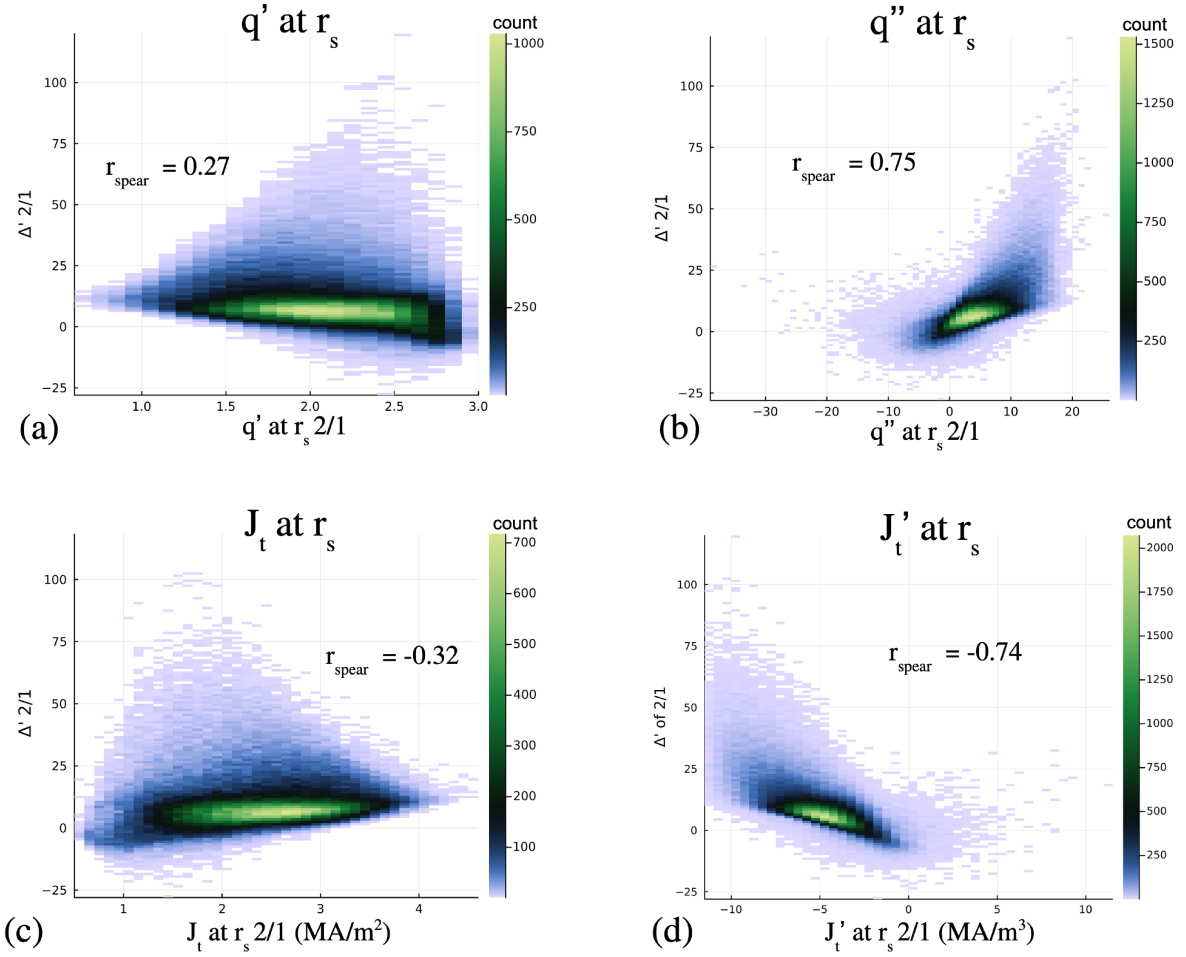

Figure 10. 2D histograms of Δ' vs magnetic shear q' (a), q'' (b), J_t (c) and J_t' (d) respectively, for 2/1 modes with $r_s > 0.3$m.

correlation with r_s. While the ideal MHD perturbation upon which Δ' depends is a function of pressure, the relatively low β values of $\sim 1\%$ can explain why there is little observable pressure-dependence.

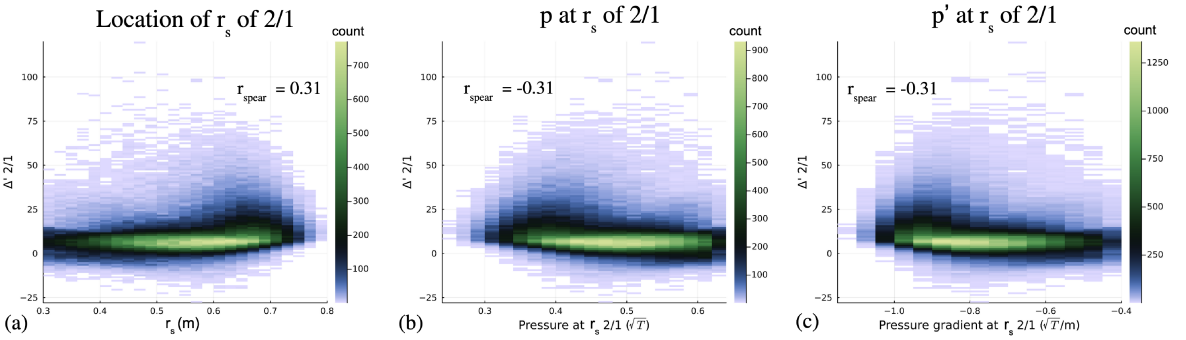

Figure 11. 2D histograms of Δ' vs the location of the rational surface r_s (a), local pressure (b) and local pressure gradient (c) respectively, for 2/1 modes with $r_s > 0.3$m.

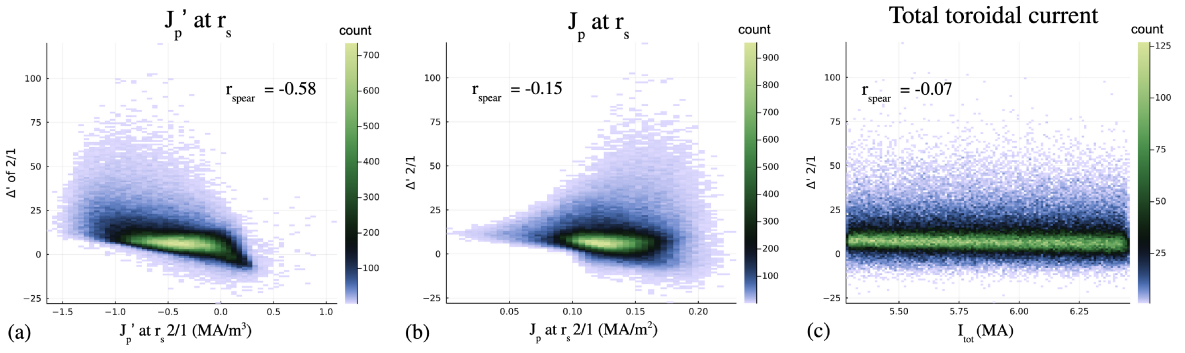

Figure 12. 2D histograms of Δ' vs local gradient of the poloidal current density J_p' (a), J_p (b) and total toroidal current I_{tot} (c) respectively, for 2/1 modes with $r_s > 0.3$m.

Figures 12a and 12b complete our analysis by showing 2D histograms of Δ' against the poloidal current density $J_p(r_s)$, $J_p'(r_s)$, and total toroidal current. $J_p'(r_s)$ has a moderate dependence with Δ', although not as strong as that of $J_t'(r_s)$ in figure 9. $J_p(r_s)$ has weak dependence with Δ' similar to $J_t(r_s)$ in figure 10c, while total toroidal current has no effect upon Δ' at all as seen in 12c.

4.1. Linear resistive MHD simulations in M3D-C1

Linear resistive MHD simulations of equilibria spanning a range of current well-depths (cases labelled in figure 13) were conducted in M3D-C1 to validate the theoretical relationship between Δ' and tearing onset in our geometry. M3D-C1 [48][49][32] is a finite-element extended-MHD code. It may be operated with varying physics-models, ranging from nonlinear 2-fluid models to linearised reduced MHD. M3D-C1's single-fluid MHD representation of magnetic and velocity fields in the cylinder is given by:

$$\mathbf{B} = \nabla\psi \times \hat{z} + B_z\hat{z}, \tag{45}$$

$$\mathbf{V} = \nabla U \times \hat{z} + \nabla\chi + V_z\hat{z}, \tag{46}$$

where scalar fields ψ, B_z, U, χ, V_z are simultaneously solved for along with pressure. M3D-C1 can operate in a reduced 2-field capacity, exclusively solving the scalar flux function ψ and incompressible velocity stream function U without evolving the other fields, removing any pressure-driven contribution to an instability. We applied both 6-field and reduced 2-field linear, single-fluid methods during simulation, to differentiate between mode growth from the pressure-driven resistive interchange, and current-driven tearing modes. Note the linear version of M3D-C1 only allows analysis of a single toroidal-mode number. The simulations were initialized with random noise in the azimuthal plane, and the resulting dominant azimuthal mode numbers were identified with visual inspection. Resistivity was set to $\eta = 9.7 \times 10^{-6}\Omega m$ and ion number density at $10^{20}m^{-3}$. [29] provides resistivity scans in a similar setup.

The pressureless simulation growth rates, displayed in figure 14, showed a 2/1 stability transition about $\Delta' = 0$ as well as a positive growth rate scaling in proportion to $(\Delta')^{4/5}$ in agreement with the linear dispersion relation (29). All pressure-evolving

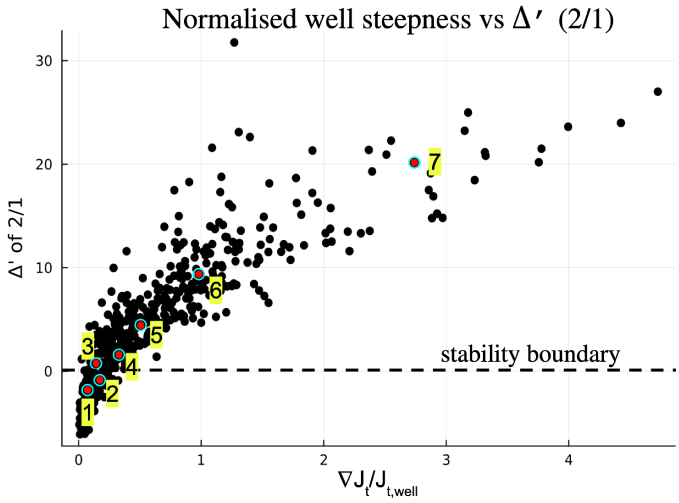

Figure 13. Current well equilibria cases simulated in M3D-C1.

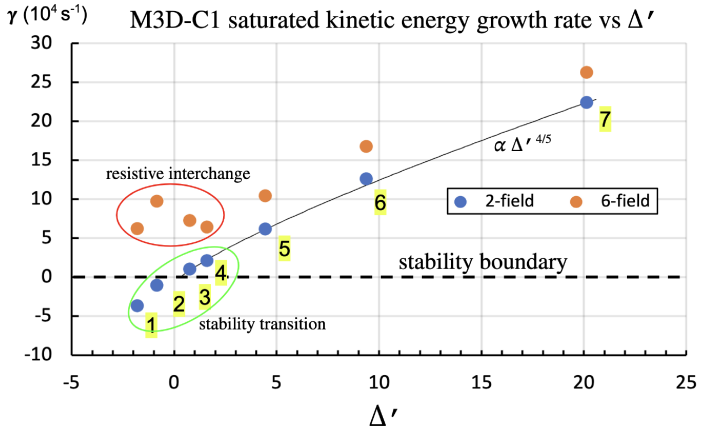

Figure 14. M3D-C1 saturated kinetic energy growth rates for the 7 current well cases labelled in figure 13, plotted against their corresponding Δ' values. The blue dots are for 2-field simulations where pressure is not evolved. The orange dots are 6-field simulations with pressure evolution present. All modes displayed 2/1 structure.

simulations were unstable to the resistive interchange as expected. These simulations confirm the validity of the Δ' analysis from section 2, in predicting the component of resistive tearing stability driven by current-profile effects. They also verify the stability transition that occurs with increasing current well-depth.

5. Summary and future work

The use of current-drive localised at the tearing rational surface has been proposed as a potential NTM stabilisation method[1][50][51], reducing NTM drive by replacing the missing bootstrap current caused by the island's presence. Our study shows that a localised current drive at the rational surface also improves linear stability via Δ', and may therefore increase seeding resistance. This observed beneficial effect of a current

hill on Δ' has been predicted for local Gaussian perturbations to the current profile [1][52][53]. In agreement with these studies, we found the stabilisation provided by the current-hill required the rational surface to be closely aligned with the hill peak ($|r_s - r_{\text{localmax}}| <\sim 8\text{mm}$).

The presence of a local current well has been found deleterious for tearing stability [15][16] in Iter baseline scenario database shots, with recent linear tearing stability runs in RDCON [54] confirming this trend. We replicate these findings in simplified cylindrical geometry. Together these results suggest that having the 2/1 rational surface in a current-well caused by the H-mode pedestal makes 2/1 tearing-onset more likely. However inclusion of toroidal and pressure effects is necessary for scenario-specific predictions.

Our MC-generated database showed that in the absence of a current-hill or well, Δ' has an approximate inverse proportionality with $J_t'(r_s)$. This could potentially explain the propensity for low m/n tearing modes ($\sim$ 3/2, 4/3) to form [21] if their rational surface lies in a region of large negative current gradient (or equivalently large q'').

The combined effects of local current hills, wells and the toroidal current gradient on Δ' have both positive and negative consequences for the application of current drive to modulate seeding resistance. If current drive can be aligned with the rational surface, either to flatten the local gradient in J_t or create a current-hill, more negative Δ' values can be achieved. However if the current-drive is misaligned to the inboard side, $J_t'(r_s)$ will become more negative driving $\Delta' > 0$ and island growth. If a small current-drive is misaligned to the outboard side, $|J_t'(r_s)|$ may be reduced, which would still benefit stability. However too great a current-drive misaligned on the outboard side will result in a local current well at r_s, driving $\Delta' > 0$ and seeding an island. In summary, although more peaked current-drive may provide greater increases in tearing-stability, the risk of the effect backfiring is greater if the accuracy requirements of r_s prediction and current deposition depth are not met at all times. For maximum passive benefit, current deposition should be aligned with key rational surfaces where possible, without applying too-sharp a deposition profile.

In line with our goal of identifying the tokamak operation & design trends that may increase resistance to NTM seeding, we will continue this work in toroidal geometry. RDCON [54] will be applied to a Monte Carlo generated database of toroidal equilibria, to analyse potential beneficial effects of shaping and mode-coupling on small-island stability.

6. Acknowledgements

The authors would like to acknowledge Commonwealth Fusion Systems for supporting this research. The simulations presented in this paper were performed on the MIT-PSFC partition of the Engaging cluster at the MGHPCC facility (www.mghpcc.org) which was funded by DoE grant number DE-FG02-91-ER54109.

7. Bibliography

[1] R. J. La Haye, Neoclassical tearing modes and their control, Physics of Plasmas 13 (5) (2006) 055501. doi:10.1063/1.2180747.
URL https://pubs.aip.org/pop/article/13/5/055501/1032332/Neoclassical-tearing-modes-and-their-controla

[2] R. Fitzpatrick, Bifurcated states of a rotating tokamak plasma in the presence of a static error-field, Physics of Plasmas 5 (9) (1998) 3325–3341. doi:10.1063/1.873000.
URL http://aip.scitation.org/doi/10.1063/1.873000

[3] R. Fitzpatrick, Helical temperature perturbations associated with tearing modes in tokamak plasmas, Physics of Plasmas 2 (3) (1995) 825–838. doi:10.1063/1.871434.
URL https://pubs.aip.org/pop/article/2/3/825/462419/Helical-temperature-perturbations-associated-with

[4] J. Wesson, D. Campbell, Tokamaks, International Series of Monographs on Physics, OUP Oxford, 2011.
URL https://books.google.com/books?id=XJssMXjHUr0C

[5] J. Freidberg, Plasma Physics and Fusion Energy, Cambridge University Press, 2008.
URL https://books.google.com.au/books?id=Vyoe88GEVz4C

[6] S. E. Wurzel, S. C. Hsu, Progress toward fusion energy breakeven and gain as measured against the Lawson criterion, Physics of Plasmas 29 (6) (2022) 062103. doi:10.1063/5.0083990.
URL https://pubs.aip.org/aip/pop/article/2847827

[7] R. J. Buttery, S. Günter, G. Giruzzi, T. C. Hender, D. Howell, G. Huysmans, R. J. L. Haye, M. Maraschek, H. Reimerdes, O. Sauter, C. D. Warrick, H. R. Wilson, H. Zohm, Neoclassical tearing modes, Plasma Physics and Controlled Fusion 42 (12B) (2000) B61. doi:10.1088/0741-3335/42/12B/306.
URL https://dx.doi.org/10.1088/0741-3335/42/12B/306

[8] Z. Chang, J. D. Callen, E. D. Fredrickson, R. V. Budny, C. C. Hegna, K. M. McGuire, M. C. Zarnstorff, Tftr Group, Observation of Nonlinear Neoclassical Pressure-Gradient–Driven Tearing Modes in TFTR, Physical Review Letters 74 (23) (1995) 4663–4666. doi:10.1103/PhysRevLett.74.4663.
URL https://link.aps.org/doi/10.1103/PhysRevLett.74.4663

[9] E. D. Fredrickson, Observation of spontaneous neoclassical tearing modes, Physics of Plasmas 9 (2) (2002) 548–559. doi:10.1063/1.1435003.
URL https://pubs.aip.org/pop/article/9/2/548/148678/Observation-of-spontaneous-neoclassical-tearing

[10] R. Buttery, T. Hender, D. Howell, R. L. Haye, O. Sauter, D. Testa, C. T. T. E.-J. Workprogramme, Onset of neoclassical tearing modes on JET, Nuclear Fusion 43 (2) (2003) 69–83. doi:10.1088/0029-5515/43/2/301.
URL https://iopscience.iop.org/article/10.1088/0029-5515/43/2/301

[11] L. Bardóczi, N. Richner, N. Logan, The onset distribution of rotating m,n=2,1 tearing modes and its consequences on the stability of high-confinement-mode plasmas in DIII-D, Nuclear Fusion 63 (12) (2023) 126052. doi:10.1088/1741-4326/ad0488.
URL https://iopscience.iop.org/article/10.1088/1741-4326/ad0488

[12] S. Gunter, G. Gantenbein, A. Gude, V. Igochine, M. Maraschek, A. M ck, S. Saarelma, O. Sauter, A. Sips, H. Zohm, T. A. U. Team, Neoclassical tearing modes on ASDEX Upgrade: improved scaling laws, high confinement at high n and new stabilization experiments, Nuclear Fusion 43 (3) (2003) 161–167. doi:10.1088/0029-5515/43/3/301.
URL https://iopscience.iop.org/article/10.1088/0029-5515/43/3/301

[13] H. P. Furth, Tearing mode in the cylindrical tokamak, Physics of Fluids 16 (7) (1973) 1054. doi:10.1063/1.1694467.
URL https://aip.scitation.org/doi/10.1063/1.1694467

[14] M. S. Chu, R. J. La Haye, M. E. Austin, L. L. Lao, E. A. Lazarus, A. Pletzer, C. Ren, E. J. Strait, T. S. Taylor, F. L. Waelbroeck, Study of a low β classical tearing mode in DIII-D, Physics of Plasmas 9 (11) (2002) 4584–4590. doi:10.1063/1.1510666.
URL http://aip.scitation.org/doi/10.1063/1.1510666

[15] F. Turco, T. Luce, W. Solomon, G. Jackson, G. Navratil, J. Hanson, The causes of the disruptive tearing instabilities of the ITER Baseline Scenario in DIII-D, Nuclear Fusion 58 (10) (2018) 106043. doi:10.1088/1741-4326/aadbb5.
URL https://iopscience.iop.org/article/10.1088/1741-4326/aadbb5

[16] F. Turco, T. C. Luce, W. Boyes, J. Hanson, A. Hyatt, Modelling and experiment to stabilize the ITER Baseline Scenario in DIII-D, Nuclear Fusion (submitted) (2024).

[17] B. Coppi, J. M. Greene, J. L. Johnson, Resistive instabilities in a diffuse linear pinch, Nuclear Fusion 6 (2) (1966) 101–117. doi:10.1088/0029-5515/6/2/003.
URL https://iopscience.iop.org/article/10.1088/0029-5515/6/2/003

[18] A. H. Glasser, J. M. Greene, J. L. Johnson, Resistive instabilities in general toroidal plasma configurations, Physics of Fluids 18 (7) (1975) 875. doi:10.1063/1.861224.
URL https://aip.scitation.org/doi/10.1063/1.861224

[19] R. Fitzpatrick, Interaction of tearing modes with external structures in cylindrical geometry (plasma), Nuclear Fusion 33 (7) (1993) 1049–1084. doi:10.1088/0029-5515/33/7/I08.
URL https://iopscience.iop.org/article/10.1088/0029-5515/33/7/I08

[20] E. C. Howell, J. R. King, S. E. Kruger, J. D. Callen, R. J. La Haye, R. S. Wilcox, Growing neoclassical tearing modes seeded via transient-induced-multimode interactions, Physics of Plasmas 29 (2) (2022) 022507. doi:10.1063/5.0076253.
URL https://aip.scitation.org/doi/10.1063/5.0076253

[21] L. Bardóczi, N. Logan, E. Strait, Neoclassical Tearing Mode Seeding by Nonlinear Three-Wave Interactions in Tokamaks, Physical Review Letters 127 (5) (2021) 055002. doi:10.1103/PhysRevLett.127.055002.
URL https://link.aps.org/doi/10.1103/PhysRevLett.127.055002

[22] R. Fitzpatrick, Stability of coupled tearing and twisting modes in tokamaks, Physics of Plasmas 1 (10) (1994) 3308–3336. doi:10.1063/1.870482.
URL https://doi.org/10.1063/1.870482

[23] A. Pletzer, A. Bondeson, R. L. Dewar, Linear Stability of Resistive MHD Modes: Axisymmetric Toroidal Computation of the Outer Region Matching Data, Journal of Computational Physics 115 (2) (1994) 530–549. doi:https://doi.org/10.1006/jcph.1994.1215.
URL https://www.sciencedirect.com/science/article/pii/S0021999184712150

[24] A. H. Glasser, Z. R. Wang, J.-K. Park, Computation of resistive instabilities by matched asymptotic expansions, Physics of Plasmas 23 (11) (2016) 112506. doi:10.1063/1.4967862.
URL https://pubs.aip.org/aip/pop/article/168307

[25] R. La Haye, C. Chrystal, E. Strait, J. Callen, C. Hegna, E. Howell, M. Okabayashi, R. Wilcox, Disruptive neoclassical tearing mode seeding in DIII-D with implications for ITER, Nuclear Fusion 62 (5) (2022) 056017. doi:10.1088/1741-4326/ac351f.
URL https://iopscience.iop.org/article/10.1088/1741-4326/ac351f

[26] J. Yang, M. Podestà, E. D. Fredrickson, C. Liu, J. W. Berkery, F. M. Poli, The role of fast ions in spontaneous neoclassical tearing mode instabilities in NSTX, Plasma Physics and Controlled Fusion 65 (6) (2023) 064004. doi:10.1088/1361-6587/acd07f.
URL https://iopscience.iop.org/article/10.1088/1361-6587/acd07f

[27] F. Waelbroeck, I. Joseph, E. Nardon, M. Bécoulet, R. Fitzpatrick, Role of singular layers in the plasma response to resonant magnetic perturbations, Nuclear Fusion 52 (7) (2012) 074004. doi:10.1088/0029-5515/52/7/074004.
URL https://iopscience.iop.org/article/10.1088/0029-5515/52/7/074004

[28] M. S. Chance, H. P. Furth, A. H. Glasser, H. Selberg, Ideal- and resistive-MHD stability of one dimensional tokamak equilibria, Nuclear Fusion 22 (1982) 187.

[29] T. Scaffidi, Stability study of the cylindrical tokamak, Tech. rep., Ecole Normale Superieure, Princeton Plasma Physics Laboratory (2011).
URL https://w3.pppl.gov/cemm/Project/Scaffidi_new.pdf

[30] P. H. Rutherford, Nonlinear growth of the tearing mode, Physics of Fluids 16 (11) (1973) 1903. doi:10.1063/1.1694232.
URL https://aip.scitation.org/doi/10.1063/1.1694232

[31] R. Sweeney, A. J. Creely, J. Doody, T. Fülöp, D. T. Garnier, R. Granetz, M. Greenwald, L. Hesslow, J. Irby, V. A. Izzo, R. J. La Haye, N. C. Logan, K. Montes, C. Paz-Soldan, C. Rea, R. A. Tinguely, O. Vallhagen, J. Zhu, MHD stability and disruptions in the SPARC tokamak, Journal of Plasma Physics 86 (5) (2020) 865860507. doi:10.1017/S0022377820001129.
URL https://www.cambridge.org/core/product/identifier/S0022377820001129/type/journal_article

[32] S. C. Jardin, N. Ferraro, J. Breslau, J. Chen, Multiple timescale calculations of sawteeth and other global macroscopic dynamics of tokamak plasmas, Computational Science & Discovery 5 (1) (2012) 014002. doi:10.1088/1749-4699/5/1/014002.
URL https://iopscience.iop.org/article/10.1088/1749-4699/5/1/014002

[33] D. Chandra, A. Sen, P. Kaw, Dynamical origin of shear flow induced modifications of magnetic islands, Nuclear Fusion 47 (9) (2007) 1238–1243. doi:10.1088/0029-5515/47/9/021.
URL https://iopscience.iop.org/article/10.1088/0029-5515/47/9/021

[34] D. Chandra, A. Thyagaraja, A. Sen, C. Ham, T. Hender, R. Hastie, J. Connor, P. Kaw, J. Mendonca, Modelling and analytic studies of sheared flow effects on tearing modes, Nuclear Fusion 55 (5) (2015) 053016. doi:10.1088/0029-5515/55/5/053016.
URL https://iopscience.iop.org/article/10.1088/0029-5515/55/5/053016

[35] A. H. Glasser, S. C. Jardin, G. Tesauro, Numerical solution of the resistive magnetohydrodynamic boundary layer equations, Physics of fluids (1994) 27 (5) (1984) 1225–1242, place: Woodbury, NY Publisher: American Institute of Physics. doi:10.1063/1.864730.

[36] W. A. Newcomb, Hydromagnetic stability of a diffuse linear pinch, Annals of Physics 10 (2) (1960) 232–267. doi:10.1016/0003-4916(60)90023-3.
URL https://linkinghub.elsevier.com/retrieve/pii/0003491660900233

[37] Y. Nishimura, J. D. Callen, C. C. Hegna, Tearing mode analysis in tokamaks, revisited, Phys. Plasmas 5 (12) (1998) 8.

[38] W. Wasow, Asymptotic expansions for ordinary differential equations, Courier Dover Publications, 2018.

[39] J. P. Freidberg, ideal MHD, Cambridge University Press, 2014.

[40] J. DeLucia, S. C. Jardin, A. H. Glasser, Resistive stability of the cylindrical spheromak, Physics of Fluids 27 (6) (1984) 1470. doi:10.1063/1.864769.
URL https://pubs.aip.org/aip/pfl/article/27/6/1470-1482/943596

[41] J. L. Johnson, J. M. Greene, Resistive interchanges and the negative V " criterion, Plasma Physics 9 (5) (1967) 611–629. doi:10.1088/0032-1028/9/5/311.
URL https://iopscience.iop.org/article/10.1088/0032-1028/9/5/311

[42] C. M. Bender, S. A. Orszag, Advanced mathematical methods for scientists and engineers I: Asymptotic methods and perturbation theory, Springer Science & Business Media, 2013.

[43] A. H. Glasser, Resistive Instabilities in a Tokamak (1975).

[44] A. H. Glasser, Z. R. Wang, Asymptotic solutions and convergence studies of the resistive inner region equations, Physics of Plasmas 27 (1) (2020) 012506. doi:10.1063/1.5134999.
URL https://pubs.aip.org/aip/pop/article/263004

[45] A. J. Creely, M. J. Greenwald, S. B. Ballinger, D. Brunner, J. Canik, J. Doody, T. Fülöp, D. T. Garnier, R. Granetz, T. K. Gray, C. Holland, N. T. Howard, J. W. Hughes, J. H. Irby, V. A. Izzo, G. J. Kramer, A. Q. Kuang, B. LaBombard, Y. Lin, B. Lipschultz, N. C. Logan, J. D. Lore, E. S. Marmar, K. Montes, R. T. Mumgaard, C. Paz-Soldan, C. Rea, M. L. Reinke, P. Rodriguez-Fernandez, K. Särkimäki, F. Sciortino, S. D. Scott, A. Snicker, P. B. Snyder, B. N.

Sorbom, R. Sweeney, R. A. Tinguely, E. A. Tolman, M. Umansky, O. Vallhagen, J. Varje, D. G. Whyte, J. C. Wright, S. J. Wukitch, J. Zhu, the SPARC Team, Overview of the SPARC tokamak, Journal of Plasma Physics 86 (5) (2020) 865860502. doi:10.1017/S0022377820001257.
URL https://www.cambridge.org/core/product/identifier/S0022377820001257/type/journal_article

[46] C. M. Bishop, Pattern recognition and machine learning, Springer, New York, 2006.

[47] G. W. Corder, D. I. Foreman, Nonparametric statistics: A step-by-step approach, John Wiley & Sons, 2014.

[48] S. C. Jardin, J. A. Breslau, Implicit solution of the four-field extended-magnetohydrodynamic equations using high-order high-continuity finite elements, Physics of Plasmas 12 (5) (2005) 056101. doi:10.1063/1.1864992.
URL https://pubs.aip.org/pop/article/12/5/056101/1015587/Implicit-solution-of-the-four-field-extended

[49] S. Jardin, J. Breslau, N. Ferraro, A high-order implicit finite element method for integrating the two-fluid magnetohydrodynamic equations in two dimensions, Journal of Computational Physics 226 (2) (2007) 2146–2174. doi:10.1016/j.jcp.2007.07.003.
URL https://linkinghub.elsevier.com/retrieve/pii/S0021999107003038

[50] L. Bardóczi, R. La Haye, E. Strait, N. Logan, S. Smith, N. Richner, J. Callen, Direct preemptive stabilization of m,n=2,1 neoclassical tearing modes by electron cyclotron current drive in the DIII-D low-torque ITER baseline scenario, Nuclear Fusion 63 (9) (2023) 096021. doi:10.1088/1741-4326/acec5c.
URL https://iopscience.iop.org/article/10.1088/1741-4326/acec5c

[51] G. Saibene, Design of the ITER electron cyclotron wave launcher for NTM control, Tech. rep., International Atomic Energy Agency (IAEA), iAEA-CN–149 (2006).
URL http://inis.iaea.org/search/search.aspx?orig_q=RN:37103064

[52] E. Westerhof, Tearing mode stabilization by local current density perturbations, Nuclear Fusion 30 (6) (1990) 1143–1147. doi:10.1088/0029-5515/30/6/017.
URL https://iopscience.iop.org/article/10.1088/0029-5515/30/6/017

[53] A. Pletzer, F. W. Perkins, Stabilization of neoclassical tearing modes using a continuous localized current drive, Physics of Plasmas 6 (5) (1999) 1589–1600. doi:10.1063/1.873412.
URL https://pubs.aip.org/pop/article/6/5/1589/104373/Stabilization-of-neoclassical-tearing-modes-using

[54] A. H. Glasser, The direct criterion of Newcomb for the ideal MHD stability of an axisymmetric toroidal plasma, Physics of Plasmas 23 (7) (2016) 072505. doi:10.1063/1.4958328.
URL http://aip.scitation.org/doi/10.1063/1.4958328